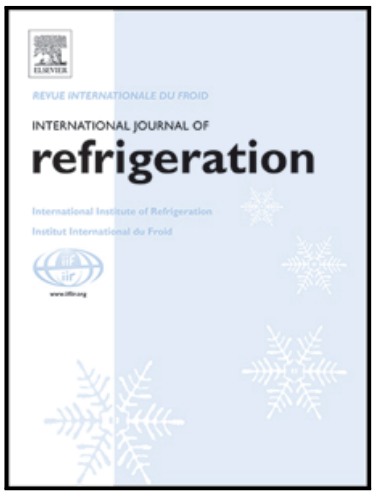

Variable speed liquid chiller drop-in modeling for predicting energy performance of R1234yf as low-GWP refrigerant

J.M. Mendoza-Miranda , C. Salazar-Hernández ,
R. Carrera-Cerritos , J.J. Ramírez-Minguela ,
M. Salazar-Hernández , J. Navarro-Esbrí , A. Mota-Babiloni

PII: S0140-7007(18)30222-6
DOI: 10.1016/j.ijrefrig.2018.06.016
Reference: JIJR 4025

To appear in: *International Journal of Refrigeration*

Received date: 3 March 2018
Revised date: 17 June 2018
Accepted date: 26 June 2018

Please cite this article as: J.M. Mendoza-Miranda , C. Salazar-Hernández , R. Carrera-Cerritos , J.J. Ramírez-Minguela , M. Salazar-Hernández , J. Navarro-Esbrí , A. Mota-Babiloni , Variable speed liquid chiller drop-in modeling for predicting energy performance of R1234yf as low-GWP refrigerant, *International Journal of Refrigeration* (2018), doi: 10.1016/j.ijrefrig.2018.06.016

Highlights

- The energy performance of liquid chiller is compared using R1234yf and R134a.
- The Buckingham π-theorem was applied to modeling drop-in.
- The predicted and experimental data are correlated in order to study the accuracy of the model.
- R1234yf shows that COP reduces about 2% -11.3% taking R134a as baseline.
- Indirect emissions are similar for R1234yf and R134a using several energy sources

Variable speed liquid chiller drop-in modeling for predicting energy performance of R1234yf as low-GWP refrigerant

J. M. Mendoza-Miranda[a,*], C. Salazar-Hernández[a], R. Carrera-Cerritos[a], J. J. Ramírez-Minguela[b], M. Salazar-Hernández[c], J. Navarro-Esbrí[d], A. Mota-Babiloni[d]

[a]*Unidad Profesional Interdisciplinaria de Ingeniería Campus Guanajuato. Instituto Politécnico Nacional. Av. Mineral de Valenciana 200 Fracc. Industrial Puerto Interior, C.P. 36275, Silao de la Victoria, Gto., Mexico.*

[b]*Departamento de Ingeniería Química, Universidad de Guanajuato, DCNE, Col. Noria Alta s/n, C.P. 36050 Guanajuato, Gto., Mexico.*

[c]*Departamento de Ingeniería en Minas, Metalurgia y Geología, División de Ingenierías Universidad de Guanajuato, Mexico.*

[d]*ISTENER Research Group, Mechanical Engineering and Construction Department, Universitat Jaume I, Campus de Riu Sec s/n, E12071, Castellon de la Plana, Spain.*

ABSTRACT

This paper presents a model for a variable-speed liquid chiller integrating a compressor model based on Buckingham π theorem to accurately predict the system performance when R134a is replaced with R1234yf, using a wide range of data obtained from an experimental setup. Relevant variables such as temperature, pressure, mass and volumetric flow rates, compressor power consumption and rotation speed were measured at several positions along the refrigeration and secondary circuits and were used to validate the developed model. Model results show that cooling capacity and power consumption predicted values are in good agreement with experimental data, within ±5%, being slightly higher for the deviation obtained for R134a than for R1234yf. Moreover, model results indicate that R1234yf has a reduction of coefficient of performance (COP) compared with R134a (between 2 and 11.3%), and that R1234yf COP reduction is diminished at intermediate volumetric flow rate and higher inlet temperature for the evaporator secondary fluid, respectively. On the other hand, an environmental analysis based on TEWI (total equivalent warming impact) method showed that direct emissions are almost negligible for R1234yf. However, there are no environmental benefits in terms of indirect greenhouse gas emissions using R1234yf without system modifications (as for instance the addition of internal heat exchanger or R1234yf new design components), which are required to reduce the liquid chiller climate change contribution using it as low GWP alternative in comparison with the typically used R134a refrigerant.

* Corresponding author
Tel. +52 (55) 57 29 6000 Ext. 81377;
E-mail: jmendozami@ipn.mx; juanmmm84@hotmail.com

Keywords: COP, hydrofuoroolefin (HFO); R134a; TEWI; vapor compression system; variable speed compressor.

NOMENCLATURE

A	Heat transfer area (m^2)	R	Fouling factor (m^2 K W^{-1})
a	Coefficients for compressor efficiencies	Re	Reynolds number
C	Constant	rp	Compression ratio
$C_{\min}$	Minimum heat transfer capacity (W K^{-1})	T	Temperature (K)
C_p	Specific heat capacity (J kg^{-1} K^{-1})	t	Average thickness of micro-fins (m)
C_r	Heat capacity rate	U	Overall HTC (W m^{-2} K^{-1})
d	Diameter (m)	$\dot{V}_b$	Volumetric flow rate (m^3 h^{-1})
e	Fin height (m)	V_G	Swept volume (m^3)
f	Friction factor	W	Compressor work (J)
F	Enhancement factor	x	Quality
g	Gravitational acceleration (m s^{-2})	***Greek symbols***	
GE	Static superheating degree (K)	α	Heat transfer coefficient (W m^{-2} K^{-1})
GR	Superheating degree (K)	β	Helix angle (rad)
GS	Subcooling degree (K)	ε	Effectiveness
h	Enthalpy (J kg^{-1})	η	Compressor efficiency
Ja	Jacob's number	π	Dimensionless parameter
		μ	Dynamic viscosity (Pa s)
k	Thermal conductivity (W m^{-1} K^{-1})	ν	Specific volume (m^3 kg^{-1})
M	Molecular weight for refrigerant used (kg $kmol^{-1}$)	ρ	Density (kg m^{-3})
$\dot{m}_{ref}$	Mass flow rate (kg s^{-1})		
n	Polytrophic constant	***Subscripts***	
N	Compressor rotation speed (rpm)	aec	Water at the inlet
N_f	Number of micro-fins	asc	Water at the outlet
N_t	Number of transverse tubes	bee	Brine at the inlet
N_r		bse	Brine at the outlet
NTU	Number of heat transfer units	i	Inlet
Nu_s	Nusselt number for smooth tube	l	Liquid
P	Pressure (kPa)	o	Outlet
Pr	Prandtl number	r	Root
Pot_c	Power consumption (W)	sec	Secondary fluid
		w	Wall
$\dot{Q}$	Thermal power (W)		

1. INTRODUCTION

In the last decades, R134a has been used instead of R12 [1] in different refrigeration and air conditioning applications for minimizing the effect on the ozone layer due to its notable energy performance, low-toxicity and non-flammable characteristics. However, through the Kyoto Protocol [2], R134a have been identified as Greenhouse Gas (GHG) as many other hydrofluorocarbons. Then, the European Parliament established a ban for fluorinated gases (F-gases) with a global warming potential (GWP) higher than 150 for their use in Mobile Air Conditioning (MAC) systems for all produced cars in 2017 [3]. In addition, in 2014, the Directive 2006/40/EC was replaced by the Regulation (EU) No 517/2014, which specified GWP limits for most extended refrigeration and air conditioning systems (2500 in stationary refrigeration equipment), and additionally stablished a progressive quota to HFCs to be placed on the market (reaching 63% reduction of the baseline 2009–2012) [4]. Consequently, it is intended that the refrigerant R134a (with zero ozone depletion potential and GWP=1450) will be replaced by other environmentally-friendly alternatives.

Therefore, two HFO (HydroFluoroOlefine) promising alternatives have been proposed: R1234yf [5] and R1234ze(E) [6], which present low-flammability, low-toxicity and GWP values of 4 and 6, respectively. In drop-in systems, R1234yf has been proposed as R134a substitute in equipment such as MAC [7] and [8], stationary refrigeration systems [9] and domestic refrigerators [10].

The development of methodologies for HFO applications in refrigeration systems has received significant attention mainly due to the possible environmental advantages obtained from the application of R1234yf and R1234ze(E) instead of R134a. For example, Lee and Jung [7] explores the drop-in performance of R1234yf in a heat pump test bencher, their results showed that the coefficient of performance (COP) of R1234yf is between 0.8 and 2.7% lower than that of R134a, and the capacity of R1234yf is up to 4% lower than that of R134a. Zilio et al. [8] conducted experiments for a compact European automotive air conditioning system with a nominal capacity of 5.8 kW. Their results showed that the TXV tuning and optimizing the compressor displacement control valve for R1234yf systems could be improved, on the other hand, simulations showed that enhancing the condenser area by 20% and the evaporator by 10%, the R1234yf showed higher COP values compared with R134a. Jarall [11] reported that cooling capacity and COP for R1234yf are lower than that obtained using R134a. Aprea et al. [10] have obtained a 3% 24h energy consumption reduction using R1234yf but Leighton et al. [12] developed a theoretical model for the steady-state analysis of a domestic refrigerator-freezer and showed that R1234yf and R1234ze(E) have lower COP and cooling capacity. Navarro-Esbrí et al. [9] experimentally studied R1234yf performance in a vapor compression system in a wide range of conditions, concluding that the cooling capacity and COP for R1234yf are about 9% and 19% lower than those obtained using R134a. Lee et al. [13] developed a theoretical model for multi-stage cycles with two-phase refrigerant injection, showing that R1234yf and R1234ze(E) have better performance than other low-GWP refrigerants. Ansari et al. [14] applied the exergy method to compare theoretically R1234yf and R1234ze(E) with R134a. They obtained that performance parameters for R1234yf are lower than those of R134a and for R1234ze(E) which are similar, concluding that both can replace R134a.

On the other hand, there is a high electric energy consumption associated with refrigeration systems, since most of these facilities are based on the vapor compression cycle. In order to study and reduce their consumption with new alternatives, the energy performance is usually assessed by one of the following approaches: (i) simplified calculations based on component characteristics; (ii) components analysis through commercial CFD packages; and (iii) standardized experiments [15]. Although the first two techniques play important roles in design, do not provide enough information on system behavior and requires previous by testing of the refrigeration system. However, experimental tests can be expensive and time consuming. A faster and less costly alternative method is the use of computer models to simulate the thermal behavior of the refrigeration systems.

Many researchers have paid attention to the development of robust and alternative approaches to modeling of vapor compression systems. For example, Browne and Bansal [16] presented a model for predicting vapor compression chiller performance using an elemental NTU-efficiency approach. Their model requires only those inputs available to the user such as condenser inlet and evaporator outlet water temperatures. Their model outputs include variables such as compressor electrical work input and COP, calculated from the refrigerant thermodynamic states. Zhou et al. [17] proposed a steady-state model of a refrigeration system for high flux removal of electronic applications and studied the effect of various external inputs and the Pareto optimization on the system performance. Their model shows good agreement between the experimental data and the model predictions.

Zhao et al. [18] developed a steady-state hybrid model of chiller, in which the compressor was modeled using a polynomial neural network and other components based in the thermodynamics first law. Based on the model, the switch point of economized and non-economized mode is investigated in detail and a linear correlation is proposed, providing a path to improve part-load energy efficiency of screw chillers. Hermes et al. [19] present a simplified model to assess the energy performance of vapor compression 'on–off' controlled refrigerators for predicting energy consumption of refrigerators and freezers. Their model use algebraic equations adjusted with experimental data obtained from the refrigeration system. This study focused to predict the energy consumption within a ±5% deviation band. On the other hand, Dalkilic and Wongwises [20] present an ideal vapor compression refrigeration system analyzing the performance of alternative mixtures for R12, R134a and R22. Their results show that the refrigeration efficiency, based on COP, increases with the evaporating temperature augmentation for a constant condensing temperature. All systems including various refrigerant blends were improved by the effect of the superheating/sub-cooling case.

Zsembinszki et al. [21] present a study of walk-in freezer refrigeration system performance under different conditions using a novel methodology for modeling a simple compression system Their model is system dependent, i.e. empirical correlations must be derived for determining some of the features of system components. Their results show that the model can accurately predict some of the main parameters of the system, such as evaporation and condensation pressures, temperature at different points of the thermodynamic cycle, and compressor consumption. Gill and Singh [22] presents the applicability of neuro-fuzzy inference system (ANFIS) to predict the COP of R134a/LPG (Liquefied Petroleum Gas) in a vapor compression refrigeration system. Their results show that the ANFIS model

predictions are in good agreement with the experiments and slightly better prediction than the mathematical models.

Given the importance of vapor compression systems modeling and to evaluate refrigerant substitution by low GWP alternatives, such as R1234yf, methods that are physical-based models or black box models integrating experimental parameters for each refrigerant tested can be considered. Therefore, the aim of this paper is to present the development of a steady-state model for the simulation of a variable speed liquid chiller applying a new approach based on Buckingham π theorem for the reciprocating compressor and to investigate the performance of this system operating with R134a and R1234yf as an alternative. This approach can reduce the number of experimental parameters to model vapor compression systems working with R134a and R1234yf. The liquid chiller model takes six input variables, namely compressor rotation speed(N), static super-heating degree at expansion valve (GE), brine inlet temperature (T_{bee}) and brine volumetric flow rate (V_{bee}) at the evaporator, and water inlet temperature (T_{aec}) and water volumetric flow rate (V_{aec}) at the condenser. These variables, coupled with the thermophysical properties of the refrigerants and the main geometric characteristics of the system, are used to calculate evaporating and condensing pressures, brine and water outlet temperatures, power consumption and coefficient of performance (COP). Finally, the energy and environmental performance of this model is tested using R1234yf and R134a as cases of study. Results can show the capabilities of this improved model for the design of variable-speed liquid chiller.

2. EXPERIMENTAL PLANT AND DATA REDUCTION

2.1 Experimental plant

The experimental test bench consists on a liquid chiller vapor compression system, and two secondary fluid circuits. The vapor compression circuit is composed by four basic components: a 5.5 kW variable speed reciprocating open type compressor using polyolester (POE) oil as lubricant, a shell and tube condenser with refrigerant flowing along the shell and water as heat dissipation fluid inside the tubes, a R134a thermostatic expansion valve, a direct expansion shell and micro-fin tube evaporator, where the refrigerant flows inside the micro-fin tubes; brine water/propylene glycol (65/35% by volume) is used as secondary fluid flowing through the shell. Figure 1 shows a diagram of the experimental facility used to develop and validate the test bench model.

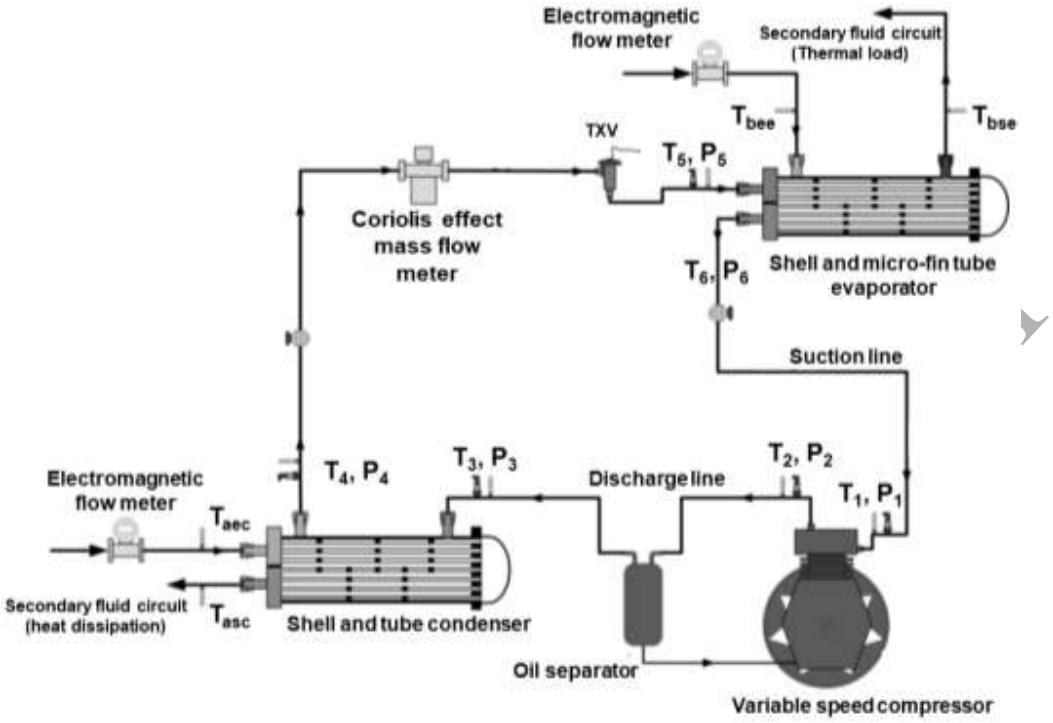

Figure 1. Schematic diagram of the test facility.

The heat dissipation water loop (condenser) consists of a closed-type cooling system, which sets the water conditions at the condenser using a commercial chiller with a variable speed pump. On the other hand, the cooling load system (evaporator) also regulates the brine water/propylene glycol temperature through a set of immersed electrical resistances driven by a Proportional-Integral-Derivative (PID) controller; meanwhile its mass flow rate can be adjusted using a variable speed pump. The variable speed compressor and the heat exchangers (evaporator and condenser) in the test bench present the main characteristics listed in Table 1 and Table 2, respectively.

Table 1. Geometrical characteristics of the compressor.

Number of cylinders	2
Piston diameter (m)	0.085
Stroke (m)	0.060
Minimum rotation speed (rpm)	400
Maximum rotation speed (rpm)	600
Displaced volume (cm^3)	681

Table 2. Main characteristics of the shell tube evaporator and condenser.

	Evaporator	Condenser
Total number of tubes	76	20
Number of tube passes	2	2
Number of Shell passes	1	1

Inner tube diameter (m)	0.00822	0.013
Outside tube diameter (m)	0.00952	0.016
No. of micro-fins	30	-
Fin height (m)	$2x10^{-4}$	-
Helix angle (°)	18	-
Inner Shell diameter (m)	0.131	0.183
Tube length (m)	0.8182	0.8
Transverse tube spacing (m)	0.01142	0.0195
Clearance between tubes (m)	0.0019	0.0035
Number of baffles	5	4

The experimental test facility is fully instrumented with sensors to measure the key variables. Table 3 lists a summary of the variables measured, as well as the sensor type and its uncertainty. All data generated by sensors were gathered by a PC-based data acquisition system and monitored with a PC.

Table 3. Measured parameters and uncertainty.

Parameter	**Sensor type**	**Uncertainty**
Temperature	K-type thermocouple	±0.3 K
Pressure	Pressure piezoelectric transducer	±0.1%
Mass flow rate	Coriolis effect mass flow meter	±0.22%
Volumetric flow rate	Electromagnetic flow meter	±0.25%
Electric power consumption	Digital wattmeter	±0.5%
Rotation speed	Inductive sensor	±1%

In the experimental study, 57 and 52 different steady-state tests using R134a and R1234yf, respectively, were conducted in a wide range of operating conditions to gather data to validate the model. The process of selecting a steady-state test consists on taking a time period of 20 min, with a sample period of 0.5 s, in which the evaporating pressure is within an interval of ±2.5 kPa. Once a steady state is achieved (with 2400 direct measurements), the data obtained was averaged over a time period of 5 min (600 measurements). Table 4 shows the R134a and R1234yf operating ranges covered by the tests.

Table 4. Operating conditions of the test bench.

	R134a	R1234yf
Volumetric flow of water at condenser ($m^3\ h^{-1}$)	1.49 – 1.75	1.67 – 1.82
Volumetric flow of brine at evaporator ($m^3\ h^{-1}$)	1.14 – 1.24	1.14 – 1.24
Temperature of brine inlet to the evaporator (K)	274.21 – 307.22	275.20– 304.28
Temperature of condensing agent (K)	290.75 – 307.22	298.82 – 327.83
Compressor rotation frequency (Hz)	35 – 50	35 – 50

2.2 Data reduction

All the measurements of pressure, temperature, volumetric flow rates, mass flow rate of refrigerant and power supplied are used to evaluate parameters such as COP, cooling capacity, condenser capacity and compressor efficiencies to characterize the steady-state performance of the system and individual components. Pressure and temperature data were used to determine the thermodynamic properties of refrigerants using REFPROP 9.1 software. Then, the calculations from the previously mentioned parameters were formulated from the mass and energy balances applied to each one of the main components of the test bench.

The experimental volumetric, isentropic and overall efficiencies for the reciprocating compressor are calculated as shown in Eqs. (1-3), respectively.

$$\eta_{v,exp} = \frac{\dot{m}_{ref,exp}}{\rho_{s,exp} V_G N_{exp}} \quad (1)$$

$$\eta_{iso,exp} = \frac{h_{2s} - h_{1,exp}}{h_{2,exp} - h_{1,exp}} \quad (2)$$

$$\eta_{all,exp} = \frac{\dot{m}_{ref,exp}(h_{2s} - h_{1,exp})}{Pot_{c,exp}} \quad (3)$$

The calculation of cooling capacity of the shell and microfin-tube heat exchanger is presented in Eq. (4) with the measured refrigerant mass flow rate and the enthalpy difference as a function of the temperature and pressure measured in the test bench, note that we assume isenthalpic process for the TXV valve, thus, the evaporator inlet enthalpy is the same than at the condenser outlet.

$$\dot{Q}_{o,exp} = \dot{m}_{ref,exp}(h_5 - h_6) \quad (4)$$

The condensing capacity in the shell and tube heat exchanger is calculated in Eq. (5), thus the enthalpies are determined as a function of the inlet and outlet pressures and temperatures for the condenser.

$$\dot{Q}_{k,exp} = \dot{m}_{ref,exp}(h_3 - h_4) \quad (5)$$

Finally, the energetic performance of the refrigeration system is evaluated by its COP, which is defined as the ratio between the experimental cooling capacity and the measured compressor power consumption.

$$COP_{exp} = \frac{\dot{Q}_{o,exp}}{Pot_{c,exp}} \quad (6)$$

3. MATHEMATICAL MODELING

The model is based on mathematical expressions arising from fundamental physics together with empirical correlations established on the basis of experimental tests. Figure 2

represents the model structure. First, the input parameters as inlet temperatures, flow rates of the secondary fluids, the compressor rotation speed and the static superheating degree are considered; and second, the model must estimate the operating pressures, outlet temperatures of secondary fluids, thermal capacitances, power consumption and the COP of the refrigeration system.

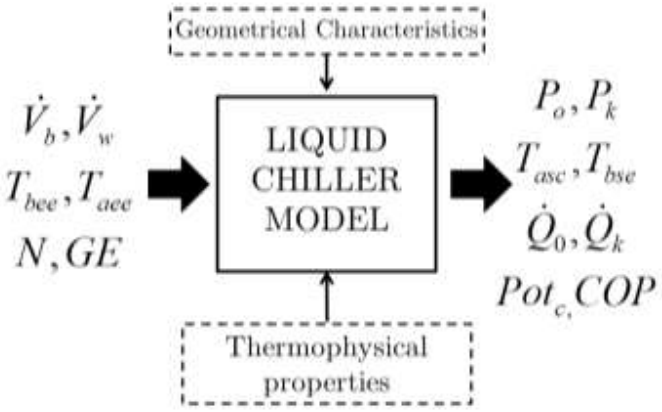

Figure 2. Input-output model structure.

For modeling, the refrigeration system was divided into three component sub-models: (i) compressor, (ii) thermostatic expansion valve, and (iii) heat exchangers (condenser and micro-fin tube evaporator). Each component sub-model is described below.

3.1 Variable speed compressor modeling

The model of a compressor can be developed through its volumetric, isentropic and overall efficiencies. Compressor efficiencies of a variable speed type mainly vary with the pressure ratio (discharge to suction pressure), as well with its rotation speed. However, the displaced volume, refrigerant type and environment temperature could have significant effects. Thus, a π-Buckingham analysis, a parametric study of dimensionless parameters and regression analyses of experimental data were carried out , allowing a confidence level of 98% and an accuracy of ±5%, ±4% and ±6% for volumetric, isentropic and overall efficiency (Eqns. 7 – 9), respectively. Table 5 shows dimensionless parameters obtained for this compressor, and the predicted results for the compressor efficiencies under the proposed model are shown in Figure 3.

$$\eta_v = \pi_2^{-0.2678}\pi_3^{-0.0106}\pi_5^{0.7195} \quad (7)$$

$$\eta_{iso} = \pi_2^{0.0753}\pi_3^{0.2183}\pi_4^{0.0015}\pi_6^{0.0972} \quad (8)$$

$$\eta_{all} = \pi_2^{-0.1642}\pi_3^{0.2050}\pi_6^{0.0659}\pi_7^{0.7669} \quad (9)$$

Table 5. Dimensionless π-numbers for volumetric, isentropic and overall efficiencies.

	Volumetric efficiency	Isentropic and overall efficiencies
π_1	η_v	$\eta_{iso}\ or\ \eta_{all}$
π_2	rp	rp
π_3	$\left[\frac{\rho_1}{P_1}\right]^{3/2} N^3 V_G$	$\frac{N_r}{N}$
π_4	$\frac{N_r}{N}$	$\frac{N^3 V_G}{\Delta h_{iso}^{3/2}}$
π_5	$\frac{M_{R134a}}{M_{alt}}$	$\frac{\Delta h_{iso}\rho_1}{P_1}$
π_6	–	$\frac{\left\lvert\frac{(T_1+T_{2,iso})}{2}-T_{amb}\right\rvert}{T_{amb}}$
π_7	–	$\frac{M_{R134a}}{M_{alt}}$

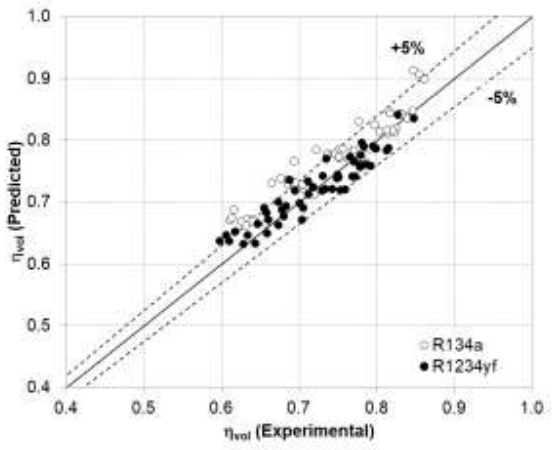

(a)

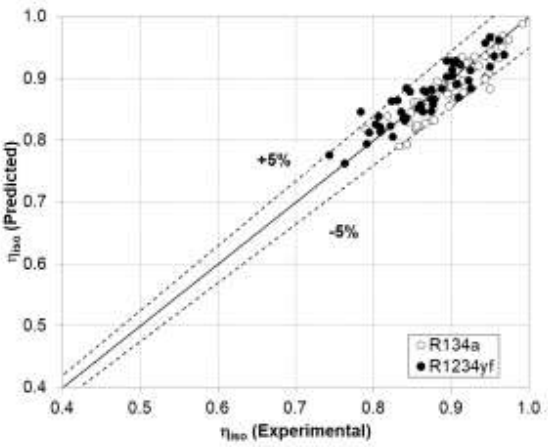

(b)

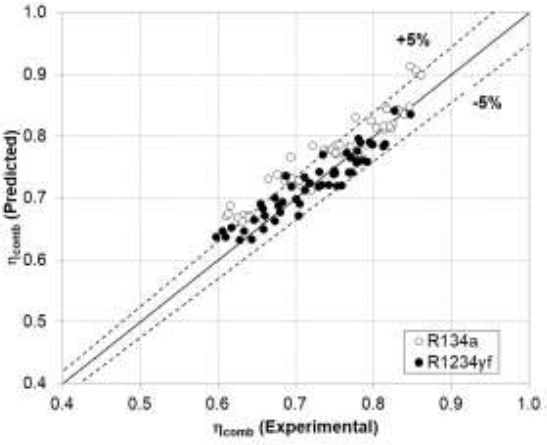

(c)

Figure 3. Calculated compressor efficiencies for R134a and R1234yf: (a) volumetric efficiency, (b) isentropic efficiency (c) combined efficiency.

Note that these compressor efficiencies expressions are valid for the operating range shown in Table 6.

Table 6. Validity range for the proposed compressor efficiencies.

	Range
Evaporating temperature (K)	260 – 280
Condensing temperature (K)	310 – 330
Suction temperature (K)	270 – 300
Compressor type	Reciprocating
Compressor rotation speed (rpm)	400 – 600
Refrigerants	R134a, R1234yf
Ambient temperature (K)	288 – 300

The refrigerant mass flow rate has been calculated using Eqn. (10).

$$\dot{m}_{ref} = \eta_v \rho_1 V_G N \tag{10}$$

The compressor discharge temperature is obtained from the isentropic efficiency, η_{iso}, and operating pressures. Thus, the refrigerant state at the compressor discharge is determined as shown in Eqn. (11).

$$h_{2r} = h_1 + \frac{(h_{2s} - h_1)}{\eta_{iso}} \tag{11}$$

The power consumption by the compressor is obtained as expressed in Eqn. (12).

$$Pot_c = \frac{\dot{m}_{ref}(h_{2s} - h_1)}{\eta_{all}} \tag{12}$$

The energetic performance of the refrigeration system is evaluated by its COP, which is defined as the ratio between the evaporator cooling capacity and the compressor power consumption (Eqn. 13).

$$COP = \frac{\dot{Q}_o}{Pot_c} \tag{13}$$

3.2 Expansion valve modeling

The thermostatic expansion valve (TXV) is modeled as an orifice through which the refrigerant expands from condensation to evaporation pressure. The flow through this component is given by Eqn. (14).

$$\dot{m}_{ref} = k_v A_0 \sqrt{2\rho_l \Delta P} \tag{14}$$

Where k_v depends on the valve aperture and on its value when the valve is fully open, and the parameter A_0 is the 'vena contracta' area. Generally, TXV manufacturer data are in terms of the refrigeration capacity or the catalog mass flow rate based on the valve fully opened parameters (Eqn. 15).

$$\sqrt{2}k_v A_0 = \frac{\dot{m}_{ref,manufacturer}}{\sqrt{\rho_l \Delta P}} \quad (15)$$

Based on experimental data for R134a and R1234yf, a general correlation for $\sqrt{2}k_v A_0$ is expressed as indicated in Eqn. (16).

$$\sqrt{2}k_v A_0 = C_1 T_{evap} + C_2 \quad (16)$$

Where C_1 and C_2 are 4.857 x10-8 m^2 C^{-1} and 2.4431x10^{-6} m^2 respectively.

Under operation, the expansion valve is partially open so that the actual mass flow rate is a fraction of the maximum value. This condition must be introduced in the model. It is known that the refrigerant mass flow rate depends both on the actual superheating degree at the outlet of the evaporator, GR, and on the static superheating degree, GE, which is a constant value of 5 K. Also, GR_{max} are obtained from manufacturer data.

$$\dot{m}_{ref} = \dot{m}_{ref,manufacturer} \frac{GR - GE}{GR_{max} - GE} \quad (17)$$

3.3 Heat exchangers modeling

The condenser and the evaporator are the components of the refrigeration system which have more influence in the thermal performance of the system, besides they have common characteristics. The following simplifications in the analysis are considered: (i) physical properties for refrigerant, secondary fluid and pipe wall are uniform in the transversal section of heat exchangers, (ii) heat exchangers are insulated, (iii) axial heat conduction in the pipes is neglected, and (iv) potential energy variations are also neglected.

For modeling, the evaporator and condenser were divided into zones that correspond to each state of the refrigerant. As a result, the evaporator was divided into two sections corresponding to refrigerant evaporation and superheating zones and the condenser has three zones, for refrigerant de-superheating, condensing and sub-cooling. Both heat exchangers are considered as two passes inside tubes heat exchangers. The ε-NTU method is used for modeling each zone. Therefore, three balance equations are used for each zone: an equation for energy balance (Eqn. 18), an equation applying the ε-NTU method (Eqn. 19) and an estimation of the wall temperature for each heat transfer area (Eqn. 20). For the completion of the evaporator modeling, the thermostatic expansion valve model is included as closing equation due to its influence on the refrigerant temperature at the evaporator outlet.

Then, the inputs are reduced to the determination of the flow rate and inlet temperature for refrigerant and secondary fluid as well as the geometrical characteristics for condenser and

evaporator (total heat transfer area). Figure 4 and 5 show the modeling process for condenser and evaporator, respectively. Thus, the primary variables to determine of the equation system are the exit and wall temperatures and the heat transfer area in each zone and the secondary ones are the condensing/evaporating pressure, outlet enthalpy, the condensing/cooling capacity, effectiveness, among other parameters.

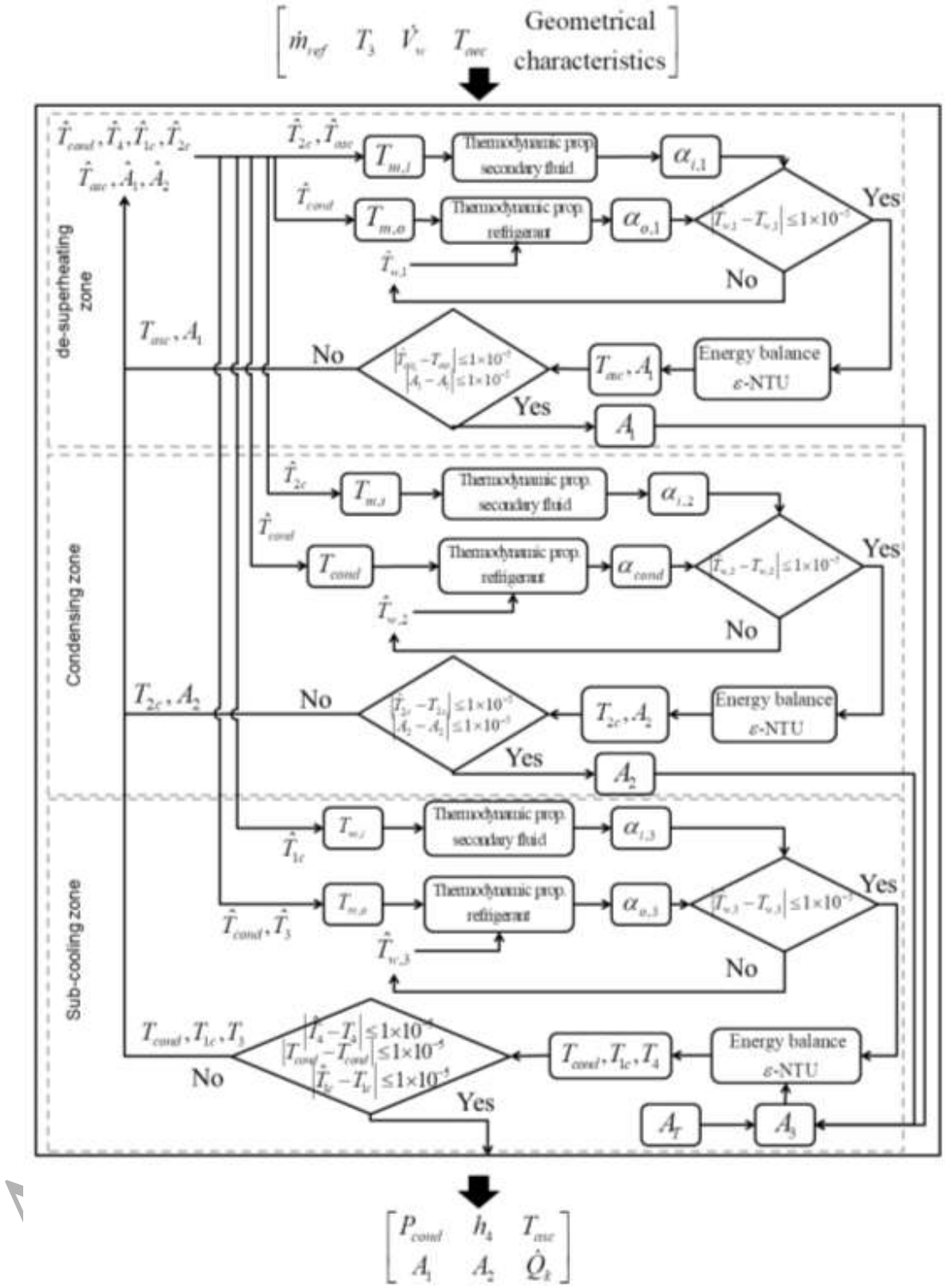

Figure 4. Condenser modeling strategy.

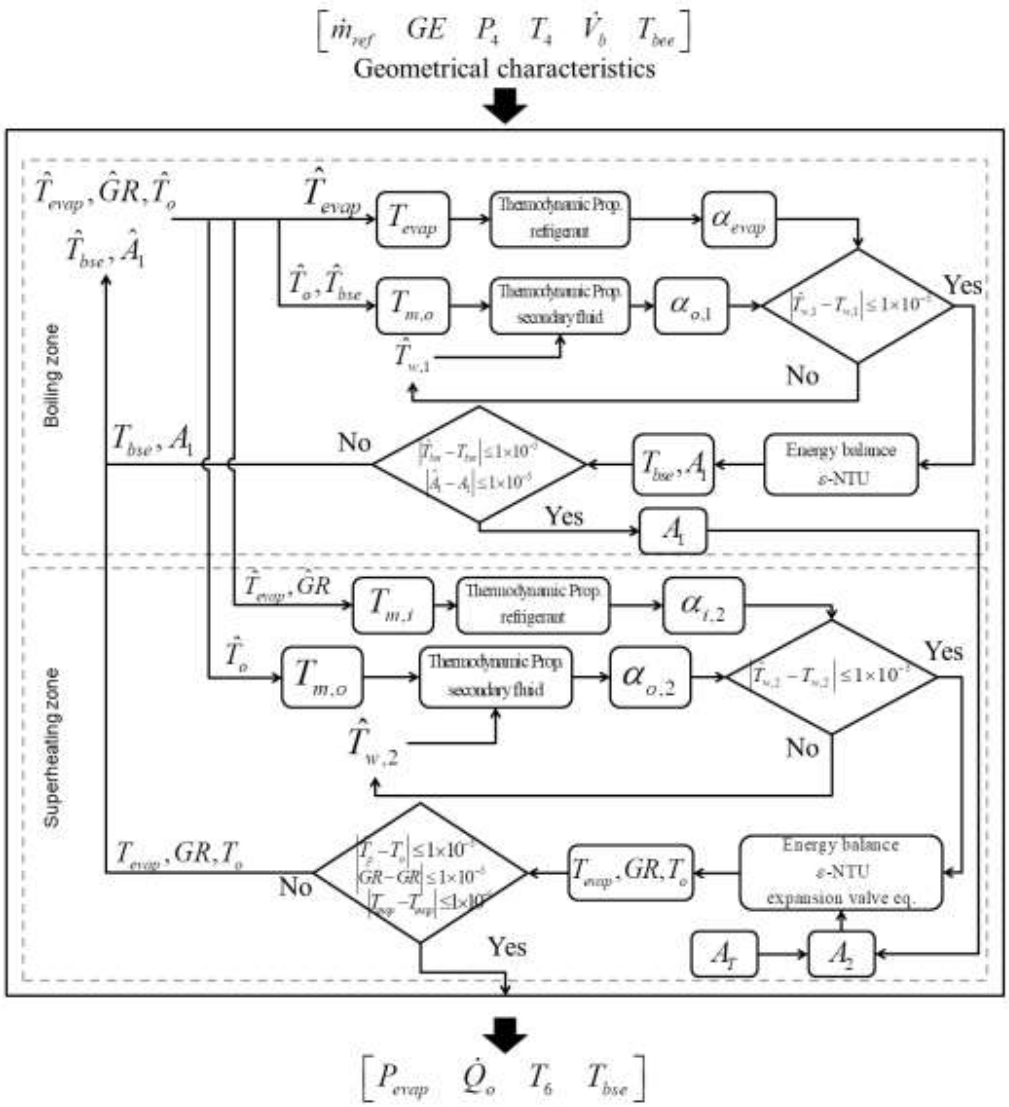

Figure 5. Evaporator modeling strategy.

$$\dot{m}_{ref}\left(h_{o,zone}-h_{i,zone}\right)-\bar{\rho}_{\sec}\dot{V}_{\sec}\bar{C}_{p,\sec}\left(T_{i,\sec}-T_{o,\sec}\right)=0 \tag{18}$$

$$\dot{m}_{ref}\left(h_{o,zone}-h_{i,zone}\right)-\varepsilon_{zone}C_{\min}\left(T_{i,\sec}-T_{i,zone}\right)=0 \tag{19}$$

$$\alpha_o A_o\left[\left(\frac{T_{i,shell}+T_{o,shell}}{2}\right)-T_{w,zone}\right]-\alpha_i A_i\left[T_{w,zone}-\left(\frac{T_{i,tube}+T_{o,tube}}{2}\right)\right]=0 \tag{20}$$

The heat exchanger effectiveness is estimated using Equations (21) and (22).

$$\varepsilon_{zone}=1-\exp\left(-NTU_{zone}\right) \qquad \text{if } C_r=0 \tag{21}$$

$$\varepsilon_{zone} = 2\left\{1 + C_r + \left(1 + C_r^2\right)^{1/2} \left[\frac{1 + \exp\left(-NTU_{zone}\left(1 + C_r^2\right)^{1/2}\right)}{1 - \exp\left(-NTU_{zone}\left(1 + C_r^2\right)^{1/2}\right)}\right]\right\}^{-1} \qquad \text{if } C_r \neq 0 \tag{22}$$

The effectiveness estimated with Eqn. (21) is for two-phase flow condition (boiling or condensing). On the other hand, for the heat transfer between two streams with no phase change, the effectiveness of the zone is estimated using Eqn. (22). The NTU parameter is defined as shown in Eqn. (23).

$$NTU_{zone} = \frac{U_{zone} A_{zone}}{C_{\min,zone}} \tag{23}$$

The overall heat transfer coefficient is calculated using Equation (24) which includes the thermal resistance associated to the fouling on the shell side in evaporator and that on tubes in condenser, $R_{o,e}$, $R_{i,c,}$ respectively. The fouling value for evaporator is 0.000086 m^2 K W^{-1} for water/propylene-glycol brine containing below 40% of propylene-glycol according to the manufacturer data, and for condenser is 0.00062 m^2 K W^{-1} considering water flowing inside the tubes.

$$U_{zone} = \left[\left(\frac{1}{\alpha_{i,zone}}\right)\left(\frac{d_o}{d_i}\right) + R_{o,e} + R_{d,i}\left(\frac{d_o}{d_i}\right) + \frac{d_o \ln\left(\frac{d_o}{d_i}\right)}{2k} + \frac{1}{\alpha_o}\right]^{-1} \tag{24}$$

3.3.1 Heat transfer coefficients

In order to calculate the heat transfer coefficients in the different flow regimes, several heat transfer correlations are used for in-tube, shell side and two-phase flows in the model (see Table 7). For single phase at evaporator in micro-fin tube side, the Jensen and Vlakancic correlation [23] is used, and at condenser the Gnielinskis' correlation [24] for smooth tubes is used, respectively. On the other hand, for two phase flow heat transfer, the Akhavan-Behabadi et al. [25] and the Jakob [26] correlations are used for in-micro-fin tube flow boiling and shell side condensation, respectively. Finally, single phase heat transfer on the shell side is calculated using Zhukauskas' correlation [27] for external forced convection on the array of tubes, where C and m coefficients, are estimated according to the Reynolds number. For two phase flow at evaporator, average heat transfer coefficient is estimated integrating the correlation between the vapor quality at the inlet and saturation quality for vapor. From the evaporator model analyzed in Mendoza-Miranda et al. [28], the best agreement with the experimental results resulted with the correlations aforementioned. The model output variables (evaporator temperatures, pressures and heat transfer) were within a ±5% bandwidth error.

Table 7. Heat transfer correlations for in-tube, shell side and two-phase flows used in the model.

Author	Int/Ext flow	Tube type and phase	Correlation
Jensen and Vlakancic	Int	Micro-fin tube single phase	$\alpha_i = \left(\frac{k}{d_i}\right) F_1^{-0.5} F_2 \left(\frac{0.25\pi d_i^2}{0.25\pi d_i^2 - N_f \cdot e \cdot t}\right)^{0.8} \mathrm{Nu}_s$ $F_1 = \begin{cases} 1-1.577\left(\frac{N_f \sin\beta}{\pi}\right)^{0.64}\left(\frac{2e}{d_i}\right)^{0.53}\left[\left(\frac{\pi}{N_f}-\frac{t}{d_i}\right)\cos\beta\right]^{0.28} & e/d_i \le 0.02 \\ 1-0.994\left(\frac{N_f \sin\beta}{\pi}\right)^{0.89}\left(\frac{2e}{d_i}\right)^{0.44}\left[\left(\frac{\pi}{N_f}-\frac{t}{d_i}\right)\cos\beta\right]^{0.41} & 0.02 < e/d_i \le 0.03 \end{cases}$ $F_2 = \left(1+\frac{2N_f \cdot e}{\pi d_i}\right)\left(1-0.059\left(\frac{N_f \sin\beta}{\pi}\right)^{-0.31}\left[\left(\frac{\pi}{N_f}-\frac{t}{d_i}\right)\cos\beta\right]^{-0.66}\right)$ $\mathrm{Nu}_s = \frac{(f/2)(\mathrm{Re}-1000)\mathrm{Pr}}{1+12.7(f/2)^{1/2}(\mathrm{Pr}^{2/3}-1)}$ $f = \left[1.58\ln(\mathrm{Re})-3.28\right]^{-2}$
Gnielinski	int	Smooth tube single phase	$\alpha_i = \frac{(f/2)(\mathrm{Re}-1000)\mathrm{Pr}}{1+12.7(f/2)^{1/2}(\mathrm{Pr}^{2/3}-1)}\left(\frac{k_f}{d_i}\right)$ $f = \left[1.58\ln(\mathrm{Re})-3.28\right]^{-2}$
Zhukauskas	Ext.	Smooth tubes bank single phase	$\alpha_o = C_1 \mathrm{Re}_{D,\max}^{m} \mathrm{Pr}^{0.36}\left(\frac{\mathrm{Pr}}{\mathrm{Pr}_w}\right)^{1/4}\left(\frac{k_f}{d_o}\right)$

Configuration	$\mathrm{Re}_{D,máx}$	C_1	m
Staggered	16 – 40	1.04	0.40
Staggered	40 – 1000	0.71	0.50
Staggered $(S_T/S_L)<2$	1000 – 2 x 10^5	$0.35(S_T/S_L)^{0.20}$	0.60
Staggered $(S_T/S_L)>2$	1000 – 2 x 10^5	0.40	0.60
Staggered	2 x 10^5 – 2 x 10^6	$0.031(S_T/S_L)^{0.20}$	0.8

Akhavan-Behabadi et al.	Int	Micro-fin tube flow boiling	$\alpha_{TP} = 4.05\times10^{-3}\,\mathrm{Re}_l^{0.98} F_\alpha^{0.38}(1.55-x)^{0.96}\left(\frac{\mathrm{Pr}_l}{X_{tt}}\right)^{1.09}$ $F_\alpha = \begin{cases} 1 & x \le 0.7 \\ 1+0.2x^{1.2}\cos(15\pi/180) & x > 0.7 \end{cases}$
Jakob	Ext	Smooth tube bank condensation	$\bar{\alpha}_{cond} = \bar{\alpha}_{Nusselt}(N_t)^{1/4}$ $\bar{\alpha}_{Nusselt} = 0.729\left[\frac{g\rho_l(\rho_l-\rho_v)k_l^3 h'_{fg}}{\mu_l(T_{sat}-T_{wall})d_o}\right]^{1/4}$ $h'_{fg} = h_{fg}(1+0.68Ja)$

$$Ja = C_{p,l}\left[\frac{T_{cond} - T_w}{h_{fg}}\right]$$

Once the characterization for each component of the test bench is completed, the models of the components were coupled to build a single representation for the overall model of the test bench. Note that the nonlinear equations system is consistent according to the number of unknown variables and equations.

4. SIMULATION PROCEDURE

The models were written in a modular format using a specific routine for each of the component sub-models. The flowchart of the vapor compression model is presented in Figure 6.

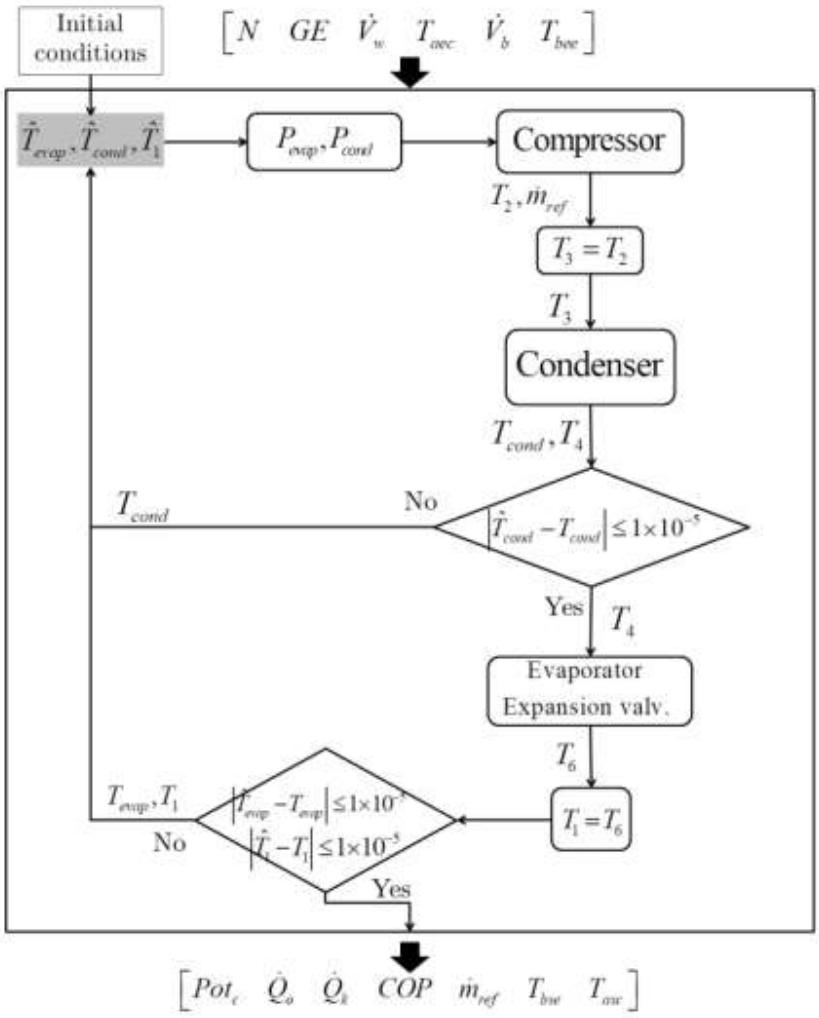

Figure 6. Variable speed liquid chiller modeling strategy.

The model needs initial guess values (arbitrarily chosen) for the calculation of the operating temperatures (such as evaporation, condensation and suction) to start the simulation. In the first step, the condensing and evaporating pressures are calculated, and then both temperatures and pressures are used in the compressor model to find the discharge temperature and mass flow rate. Using these values, the discharge line and condenser conditions are obtained. The condensing temperature is compared with the initial one and if the difference is greater than $1x10^{-5}$, the guessing condensing temperature is updated according to the governing equations and the process is repeated. Otherwise, if the difference is lower than $1x10^{-5}$, the evaporator model is solved and now the comparison is made with the evaporation and suction temperatures. When both differences are lower than $1x10^{-5}$, the guess values of the parameters satisfy the established restrictions of convergence and the resulting values are considered accurate enough, and hence, they are taken as outputs of the model.

5. RESULTS AND DISCUSSION

5.1 MODEL VALIDATION

Figures 7 – 10 show comparisons between measured and predicted data for the two tested refrigerants (R134a and R1234yf). Figure 7 highlights the measured mass flow rate and those calculated with the proposed volumetric efficiency correlation. It can be seen that the results highly agree, within ±5% of error bandwidth for both R134a and R1234yf.

Figure 8 shows the measured operating pressures compared with those obtained using the model. It can be seen that all the results are within ±5% of the measured values. In the model, a good prediction of evaporating pressure is observed for both refrigerants. On the other hand, all the predicted condensing pressure data agree quite well with the tested data (Figure 8b). However, most of the deviations are slightly higher for R134a than those obtained for R1234yf, corresponding to low and high condensing pressures reaching up to ±5% of error bandwidth.

Figure 9 shows a comparison between the measured and predicted values for the cooling capacity, Q_o, and the thermal load removed at condenser, Q_k, are within an error bandwidth of ±5%. The values of the cooling capacity and the thermal load removed used are obtained from the refrigerant side measurements, which coincide with the values obtained from the brine side. Furthermore, predicted values of the compressor power consumption and COP, can be compared with those obtained with the experimental setup. In this case, as it can be observed from Figure 10, in most of experimental test the model error is also within ±5%.

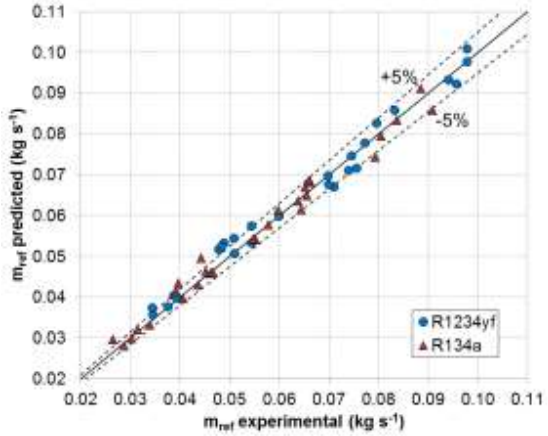

Figure 7.Validation of refrigerant mass flow rate.

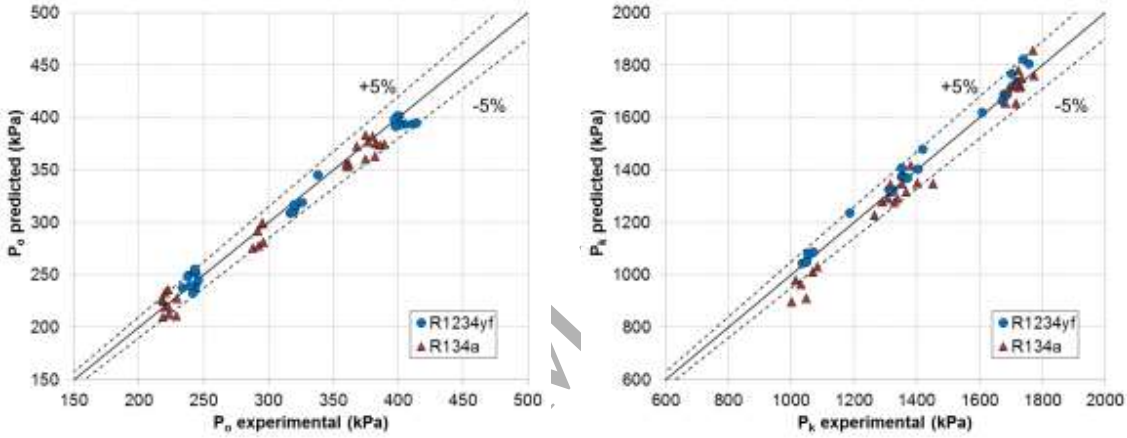

(a) (b)

Figure 8.Validation of (a) evaporating pressure, (b) condensing pressure.

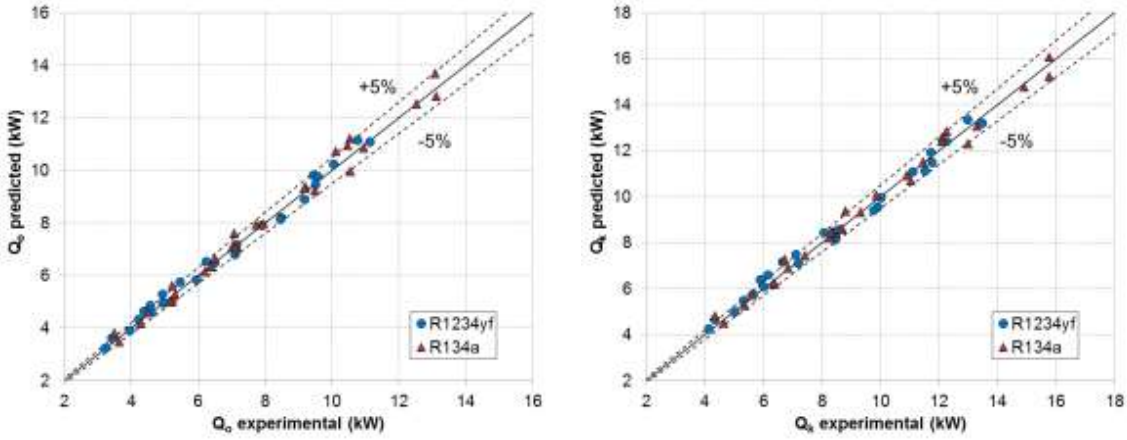

(a) (b)

Figure 9.Validation of (a) cooling capacity, (b) condenser capacity.

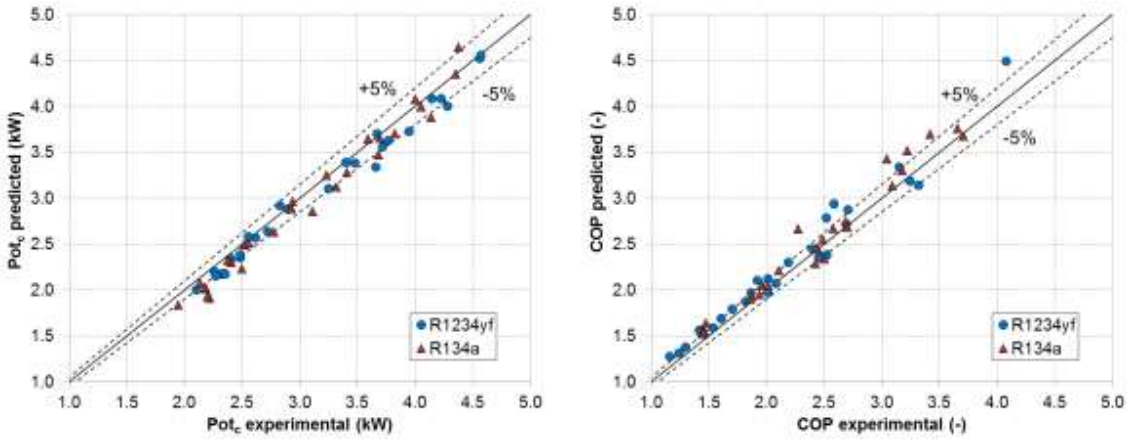

(a) (b)

Figure 10. Validation of (a) power consumption (b) coefficient of performance, COP.

5.2 Energy performance evaluation

The described model is now applied to a large set of input values combinations to observe the system efficiency behavior when the main operating conditions are varied using R134a and R1234yf. This section summarizes the results obtained using the proposed model to simulate a variable speed vapor compression chiller performance.

Firstly, it the influence of the main operating variables in COP is studied. The volumetric flows and temperatures at condenser and micro-fin tubes evaporator influence on the global coefficient of performance (COP) are presented in Figure 11.

Figures 11a and 11b show the influence on COP of the condenser secondary fluid varying the volumetric flow and the temperature. It can be observed that COP strongly decreases when the temperature increases. For instance, at 575 rpm, the COP increases about 13% when volumetric flow increases from 1 to 2 m^3 h^{-1} using R134a and about 19% using R1234yf (Figure 11a). In the same way, if the secondary fluid inlet temperature at condenser varies, COP shows an approximate decrease of 48% using R134a; meanwhile for R1234yf the COP decreases about 52%. On the other hand, maintaining the same operating conditions for a compressor speed of 400 rpm, the COP decreases between 3 and 9% when R134a is replaced by R1234yf under low compressor speed (400 rpm), meanwhile if the compressor speed is raised to 575 rpm, the COP shows a decrease of 5 to 8% replacing R134a using R1234yf.

The decrease in the COP is affected by a rise in the pressure ratio (the temperature of condensation increases), producing major power consumption, lower compressor efficiencies, and a decrease in the cooling capacity due to the higher quality of the refrigerant at the evaporator inlet. On the other hand, the volumetric flow of secondary fluid causes an increase of COP due to the increase in condenser sub-cooling for refrigerant, therefore, the quality at the inlet of evaporator decreases and then, the cooling capacity increase, taking into account that the changes in pressure and power consumption are not

significant. Thus, the inlet temperature has a major influence in the COP than the secondary volumetric flow at condenser.

When the volumetric flow varies at evaporator (Figure 11c), the brine volumetric flow rate has a slightly more influence on COP than water volumetric flow rate in the studied range for these variables. Thus, using R134a, a rotation speed of 575 rpm and increasing the brine volumetric flow at evaporator from 0.6 $m^3 h^{-1}$ to 1.2 $m^3 h^{-1}$; it is observed a COP increase of 40%. In the other hand, for the same operating conditions but using R1234yf, COP increases 33%. The COP decreases about 4.6% at low compressor rotation speed and up to 9.5% at high values when R1234yf is used in the liquid chiller. The increase in the COP with the secondary fluid volumetric flow rate at evaporator is due by the adjustment in the cooling capacity demand causing an increase in the evaporating pressure, and hence, the power consumption decreases by the lower pressure ratio at compressor.

The influence of brine temperature on the COP is studied in Figure 11d. For R134a, the COP increases about 50% when the brine temperature increases from 270 to 295 K. In the same way, for R1234yf and the same operating conditions, COP increases about 63%. It is observed that the COP varies significantly with the brine inlet temperature. Replacing R134a, the observed decrease in COP lies between 5.7 and 7.8% at low compressor rotation speed and when it is 575 rpm, COP decreases between 9.1 and 11.8%. Note that for high brine temperatures R1234yf tend to approach R134a COP. The effect of the secondary fluid temperature has the opposite effect observed for the condenser, that is, there is a decrease in the pressure ratio and power consumption.

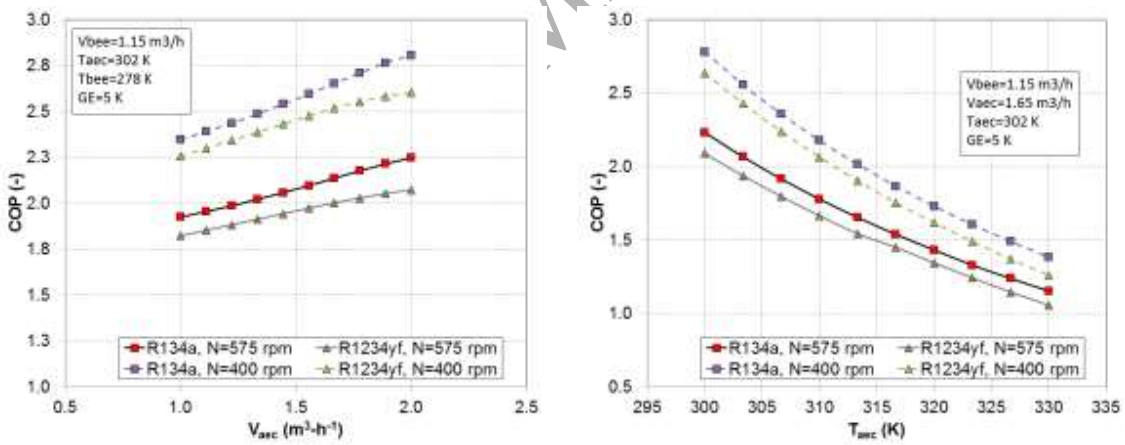

(a) (b)

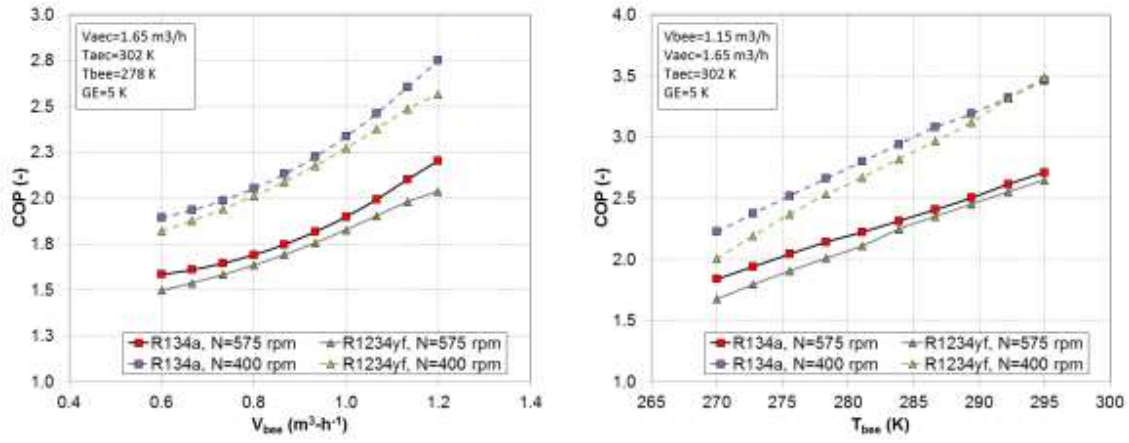

(c) (d)

Figure 11. COP vs operating conditions at condenser and evaporator at different compressor rotation speed using R134a and R1234yf, varying (a) volumetric flow rate at condenser, (b) water temperature at condenser inlet, (c) brine volumetric flow at evaporator, (d) brine temperature at the inlet of evaporator.

Finally, Figure 12 shows the behavior of the COP when the compressor rotation speed is varied. Analyzing the compressor rotation speed, COP decrease at high compressor rotation speed. For the same system and using R1234yf, it is observed a decrease of COP between 4 to 11% when the compressor rotation speed varies and comparing the same operating conditions when R134a is used. The decrease in COP when the rotation speed increases is due to the direct relation between refrigerant mass flow rate and compressor suction and discharge pressure drops that causes a reduction in the compressor efficiencies.

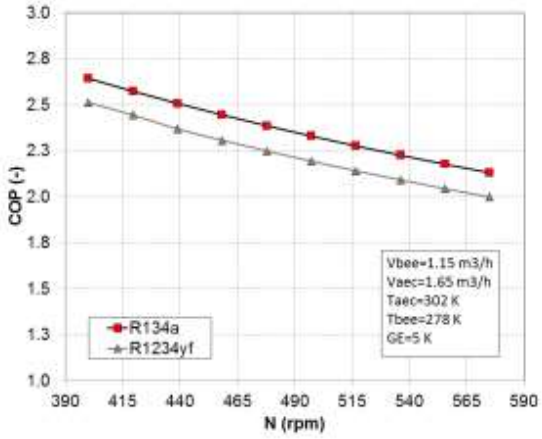

Figure 12. COP vs compressor rotation speed.

From Figures 11 and 12, it can be seen that the best conditions for R134a replacement using R1234yf is at higher secondary fluid evaporator inlet temperature and lower rotational speed. At these conditions, the R1234yf power consumption increase compared to that of R134a is reduced and COP of both fluids can be considered comparable. Additionally, R1234yf thermodynamic properties show more similarity to R134a at high temperatures or pressures.

5.3 Environmental impact using TEWI analysis

The total equivalent warming impact (TEWI) was developed as a measure of the direct and indirect global warming impacts of the refrigerant losses to the atmosphere and the CO_2 emissions from energy source to generate power to run the vapor compression system. Maykot et al. [29] defined TEWI in equivalent of kg·CO_2 as shown in Equation (15).

$$TEWI = GWP \cdot L \cdot n + GWP \cdot m \cdot (1-\gamma) + n \cdot E \cdot \lambda \quad (15)$$

Equation (15) considers system refrigerant leakages, recuperation losses and energy consumption. Detailed information about these parameters can be found in Makhnatch and Khodabandeh [30]. For the environmental evaluation of the liquid chiller, Table 8 summarizes two different operating conditions and the amount of energy consumption of both R134a and R1234yf for the same secondary fluid conditions. The emission factor relationship between electricity generation and CO_2 production vary significantly, depending on the approach to be followed. Here, the average emission factor is taken from Maykot et al. [29], who provides several primary energy sources based on a Life Cycle approach. These values were used by these authors to evaluate TEWI analysis for refrigerant replacement in household and commercial applications for different locations.

Figure 13 shows the resulting TEWI for both refrigerants using different energy sources in tons of equivalent CO_2 (t CO_2-eq.). As can be appreciated in Figure 13a, the TEWI for R1234yf is 3.5% lower than R134a due to almost negligible direct emissions for R1234yf (GWP value close to the unity). However, the resulting TEWI, when only considering GHG emission by energy consumption, for this alternative was approximately 2% higher than R134a, and there are no environmental benefits without system modifications in this case (Figure 13b). R1234yf is disadvantaged by a COP reduction at most conditions observed. Besides, warming impact due by the system operation could be reduced depending of the primary energy sources (Figure 13a) and R1234yf utilization is benefited from clean energies as nuclear or renewable technologies that reduces the significance of the energy performance of the refrigeration system. If the production of electricity using this kind of technologies is not possible, an improvement of the energy performance of actual system is required to improve the liquid chiller environmental effect (Figure 13b). This can be achieved considering, for instance, system modifications like the introduction of an internal heat exchanger, components specifically designed and sized for R1234yf operation, consideration of other compressor technologies, better super-heating and sub-cooling adjustment, or oversized condenser, among others.

Table 8. Refrigeration system operating conditions selected for the TEWI analysis.

	Case A Constant compressor speed		Case B Variable speed			
Compressor rotation speed (rpm)	575		400		575	
Refrigerant	R134a	R1234yf	R134a	R1234yf	R134a	R1234yf
Volumetric flow of water at condenser ($m^3 h^{-1}$)	1.65	1.65	1.65	1.65	1.65	1.65
Volumetric flow of brine at evaporator ($m^3 h^{-1}$)	1.15	1.15	1.15	1.15	1.15	1.15
Temperature of condensing agent (K)	302	302	302	302	302	302
Temperature of brine inlet to the evaporator (K)	278	278	278	278	278	278
Static superheating degree (K)	5	5	5	5	5	5
Power consumption (kW)	2.90	3.01	1.84	1.89	2.90	3.01
Refrigerant charge (kg)	8	8	8	8	8	8
Operation time (h/day)	6	6	2.5	2.5	6	6

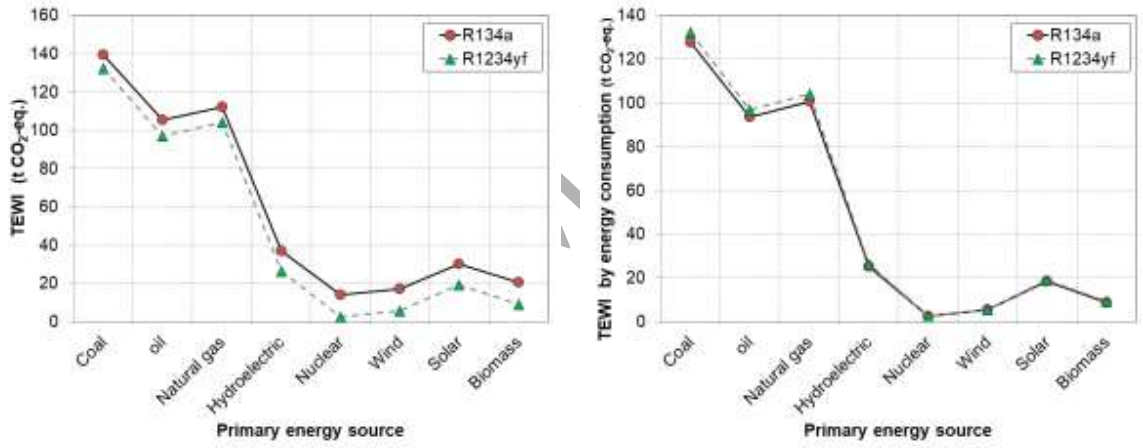

(a) (b)

Figure 13. Total Equivalent Warming Impact using different energy sources considering (a) indirect and direct emissions, (b) only indirect emissions due to energy consumption.

6. CONCLUSIONS

In this paper, a model of a variable-speed liquid chiller has been proposed. This model is based on a steady state physical laws making use of low cost data, and employing the dimensionless analysis for refrigerant replacement, which can be easily obtained from an existing liquid chiller. The input parameters of the model are the inlet characteristics of the secondary fluids and the compressor rotation speed, giving as model outputs, the operating pressures, secondary fluids output variables and the system overall energy performance. The results for the studied experimental tests show that the proposed model is able to accurately predict the steady state system operation and energy performance with errors below 5% for R134a and R1234yf.

The model has been used to analyze the R134a and R1234yf system behavior in different operating conditions in order to be used for energy performance calculation by changing the operating parameters, such as compressor speed, secondary fluids input temperatures, and volumetric flow rates. The energetic comparison is performed on the basis of the COP obtaining that R1234yf reduces the COP of the refrigeration system from 2% to 11.3% compared to that obtained using R134a and depending on the input variables that are modified.

For the range of values of the given variables, the model results show that the main driving magnitudes are compressor speed and secondary fluids inlet temperatures, whereas brine and water volumetric flow rates have a lower influence on global system efficiency, but they must also be tuned to reduce energy consumption.

Finally, direct emissions are negligible for R1234yf due to its GWP value close the unity; its resulting TEWI only caused by energy consumption was approximately 2% higher than that of R134a and there are no environmental benefits without system modifications, thus, system modifications are required to improve the liquid chiller environmental effect.

7. ACKNOWLEDGEMENTS

The authors are grateful to ISTENER research group of University Jaume I, for their partial support on this study. The linguistic support of Irene I. Elias-Miranda is appreciated. Adrián Mota-Babiloni acknowledges the Spanish Government for the financial support through the grant “Juan de la Cierva-formación 2016” (FJCI-2016-28324) and Universitat Jaume I through the grant “Becas Iberoamérica. Santander Investigación. Santander Universidades (Convocatoria 2017-2018)” (17I213).

REFERENCES

[1] E. Halimic, D. Ross, B. Agnew, A. Anderson and I. Potts, "A comparison of the operating performance of alternative refrigerants," *Applied Thermal Engineering,* vol. 23, pp. 1441-1451, 2003.

[2] Kyoto Protocol, "Report of the conference of the parties," in *United Nations Framework Convention on Climate Change (UNFCCC)*, 1997.

[3] "Directive 2006/40/EC of The European Parliament and of the Council of 17 May 2006 relating to emissions from air-conditioning systems in motor vehicles and amending Council Directive 70/156/EC," *Official Journal of the European Union,* 2006.

[4] "Regulation (EU) No 517/2014 of the European Parliament and the Council of 16 April 2014 on fluorinated greenhouse gases and repealing Regulation (EC) No 842/2006," *Official Journal of*

the European Union, 2014.

[5] B. Minor and M. Spatz, "A low refrigeran for MAC," in *"nd International Workshop on Mobile Air Conditioning and Auxiliary Systems*, Torino, Italy, 2007.

[6] "Honeywell International Inc, "Solstice™ ze (HFO-1234ze) Refrigerant. The environmental alternative to traditional refrigerants," 2012. [Online]. Available: http://www.honeywell-refrigerants.com/india/?document=solstice-ze-hfo-1234ze-brochure-2012&download=1. [Accessed 28 May 2015].

[7] Y. Lee and D. Jung, "A brief performance comparison of R1234yf and R134a in a bench tester for automobile applications," *Applied Thermal Engineering,* vol. 35, pp. 240-242, 2012.

[8] C. Zilio, J. S. Brown, G. Schiochet and A. Cavallini, "The refrigerant R1234yf in air conditioning systems," *Energy,* vol. 36, no. 10, pp. 6110-6120, 2011.

[9] J. Navarro-Esbrí, J. M. Mendoza-Miranda, A. Mota-Babiloni, A. Barragán-Cervera and J. M. Belman-Flores, "Experimental analysis of R1234yf as a drop-in replacement for R134a in a vapor compression system," *International Journal of Refrigeration,* vol. 36, no. 3, pp. 870-880, 2013.

[10] C. Aprea, A. Greco and A. Maiorino, "An experimental investigation on the substitution of HFC134a with HFO1234YF in a domestic refrigerator," *Applied Thermal Engineering,* pp. 959-967, 2016.

[11] S. Jarall, "Study of refrigeration systemwith HFO-1234yf as working fluid," *International Journal of Refrigeration,* vol. 35, pp. 1668-1677, 2012.

[12] D. Leighton, Y. Hwang and R. Radermacher, "Modeling of household refrigerator performance with low global warming potential alternative refrigerants," *ASHRAE Transactions,* vol. 118, pp. 658-665, 2012.

[13] H. Lee, H. Wang, R. Radermacher and H. Chun, "Potential benefits of saturation cycle with two-phase refrigerant injection," *Applied Thermal Engineering,* vol. 56, pp. 27-37, 2013.

[14] N. Ansari, B. Yadav and J. Kumar, "Theoretical exergy analysisof HFO-1234yf and HFO-1234ze as an alternative replacement of HFC-134a in simple vapour compression refrigeration system," *Int. J. Sci. Eng. Res. ,* vol. 4, pp. 137-144, 2013.

[15] J. M. Goncalves, C. Melo and C. J. Hermes, "A semi-empirical model for steady-state simulation of hoseholdrefrigerators," *Applied Thermal Engineering,* vol. 29, pp. 1622-16-30, 2009.

[16] M. W. Browne and P. K. Bansal, "An elemental NTU-ε model for vapour-compression liquid chillers," *International Journal of Refrigeration,* vol. 24, no. 7, pp. 612-627, 2001.

[17] R. Zhou, T. Zhang, J. Catano, J. T. Wen, G. J. Michna and Y. Peles, "The steady-state modeling and optimization of a refrigeration system for high heat flux removal," *Applied Thermal Engineering,* vol. 30, pp. 2347-2356, 2010.

[18] L.-X. Zhao, L.-L. Shao and C.-L. Zhang, "Steady-state hybrid modeling of economized screw water chillers using polynomial neural network compressor model," *Internationa Journal of Refrigeration,* vol. 33, pp. 729-738, 2010.

[19] C. J. Hermes, C. Melo, F. T. Knabben and J. M. Gonçalves, "Prediction of the energy consumption of household refrigerators and freezers via steady-state simulation," *Applied Energy,* vol. 86, pp. 1311-1319, 2009.

[20] A. S. Dalkilic and S. Wongwises, "A performance comparison-compression refrigeration system using various alternative refrigerants," *International Communications in Heat and Mass Transfer,* vol. 37, pp. 1340-1349, 2010.

[21] G. Zsembinszki, A. de Gracia, P. Moreno, r. Rovira, M. Á. Gozález and L. F. Cabeza, "A novel numerical methodology for modelling simple vapour compression refrigeration system," *Applied Thermal Engineering,* vol. 115, p. 188 – 200, 2017.

[22] J. Gill and J. Singh, "Performance analysis of vapor compression refrigeration system using an adaptive neuro-fuzzy inference system," *International Journal of Refrigeration,* vol. 82, pp. 436-446, 2017.

[23] M. Jensen and A. Vlakancic, "Technical note - experimental investigation of turbulent heat transfer and fluid flow in internally finned tubes," *International Journal of Heat and Mass Transfer,* vol. 42, pp. 1343-1351, 1999.

[24] V. Gnielinski, "New equations for heat and mass transfer in turbulent pipe and channel flow," *Int. Chem. Eng.,* vol. 16, pp. 359-368, 1976.

[25] M. A. Akhavan-Behabadi, S. G. Mohseni and S. M. Razavinasab, "Evaporation heat transfer of R-134a inside a microfin tube with different tube inclinations," *Experimental Thermal and Fluid Science,* vol. 35, pp. 996-1001, 2011.

[26] M. Jakob, Heat Transfer, vol. 1, New York: Wiley, 1949.

[27] A. Zhukauskas, "Heat transfer from tubes in cross flow," in *Advances in Heat Transfer*, New York, Academic Press, 1972.

[28] J. M. Mendoza-Miranda, J. J. Ramírez-Minguela, V. D. Muñoz-Carpio and J. Navarro-Esbrí, "Development and validation of a micro-fin tubes evaporator model using R134a and R1234yf as working fluids," *International Journal of Refrigeration,* vol. 50, pp. 32-43, 2015.

[29] R. Maykot, G. C. Weber and R. Maciel, "Using the TEWI Methodology to evaluate Alternative Refrigeration Technologies," in *International Refrigeration and Air Conditioning Conference*, Purdue University, 2004.

[30] P. Makhnatch and R. Khodabandeh, "he Role of Environmental Metrics (GWP, TEWI, LCCP) in the Selection Of Low GWP Refrigerant," *Energy Procedia,* vol. 61, pp. 2460-2463, 2014.